AIAA JOURNAL
Vol. 33, No. 6, June 1995

Some Aspects of High-Speed Blunt Body Flow Computations with Roe Scheme

S. K. Saxena* and K. Ravi†
National Aerospace Laboratories, Bangalore 560017, India

This paper discusses some aspects of three-dimensional supersonic and hypersonic inviscid blunt body flow computations. The mehtod used is based on the solution of the Euler equations employing an explicit, upwind total variation diminishing formulation of the Roe Riemann solver within the cell-centered finite volume approach. A comparative study of various total variation diminishing limiters and entropy fixes is carried out to identify the most appropriate combination. The effect of using cell spacing in the total variation diminishing extrapolations is highlighted. Furthermore, a Mach number dependence and grid sensitivity study is carried out on various total variation diminishing limiters scaled with mesh spacing. Local time stepping and code parallelization has been employed to accelerate convergence in terms of effective wall clock times.

Introduction

THE knowledge of the aerodynamic loads experienced by space vehicles at supersonic and hypersonic speeds is crucial for its successful design. These high-speed configurations are invariably designed to have a blunt forebody due to heating rate considerations. The flowfield of such blunt bodies is characterized by a strong detached bow shock and a thin shock layer with a subsonic pocket in the nose region. The computation of such a flowfield is a challenging task.

As part of a program to compute such flows, a robust flow solver has been developed based on the solution of three-dimensional time-dependent Euler equations with ideal gas assumption. An explicit high resolution total variation diminishing (TVD) scheme employing Roe's Riemann solver has been formulated within the finite volume framework. The aim of this paper is to study, numerically, the effect of various entropy fixes and TVD limiters on accuracy, convergence, and stability of computations for three-dimensional blunt body high-speed flows. Roe's approximate Riemann solver does not satisfy entropy condition at the sonic rarefactions, and this results in expansion shocks. Anomalies for high Mach number flows as well as entropy violation are also observed. Various formulations of entropy fixes are investigated in this paper.

The use of TVD limiters is essential in capturing strong blunt body shocks without wiggles. These limiters, however, are known to affect convergence. A study of various limiters on nonuniform grids has been undertaken by extending them to take into account cell center distances. This modification dramatically improves convergence. The effect of Mach number dependence and grid refinement on the performance of TVD limiters is also studied. To the knowledge of the authors, such a study has not been attempted in the past for three-dimensional blunt body flows. Local time stepping and parallelization techniques are employed to accelerate convergence. In each case, a full three-dimensional axisymmetric grid is used with no symmetry boundary conditions.

Governing Equations

The nondimensionalized Euler equations cast in strong conservation law form in generalized body-fitted coordinates can be written as

$$\frac{\partial \hat{Q}}{\partial \tau} + \frac{\partial \hat{F}}{\partial \xi} + \frac{\partial \hat{G}}{\partial \eta} + \frac{\partial \hat{H}}{\partial \zeta} = 0 \tag{1}$$

For the transformation

$$\tau = t, \qquad \xi = \xi(x, y, z)$$
$$\eta = \eta(x, y, z), \qquad \zeta = \zeta(x, y, z) \tag{2}$$

where

$$\hat{Q} = \frac{1}{J}\begin{pmatrix} e \\ \rho \\ \rho u \\ \rho v \\ \rho w \end{pmatrix} \qquad \hat{E} = \frac{1}{J}\begin{pmatrix} (e+p)W \\ \rho W \\ \rho u W + p\kappa_x \\ \rho v W + p\kappa_y \\ \rho w W + p\kappa_z \end{pmatrix} \tag{3}$$

$Q = J\hat{Q}$ is the state vector of conserved variables, and J is the Jacobian of the transformation. The contravariant velocity is given by $W = u\kappa_x + v\kappa_y + w\kappa_z$. For the vectors $\hat{F}$, $\hat{G}$, and $\hat{H}$, $\kappa = \xi, \eta$, and ζ, respectively. The Cartesian velocity components are u, v, and w, respectively, and the velocity vector $U = u\hat{i} + v\hat{j} + w\hat{k}$ with $q^2 = U \cdot U$. The fluid density is ρ. The total energy per unit volume is $e = \rho I + 1/2\rho q^2$ where I is the internal energy per unit mass of the gas. The pressure p is given by the equation of state $p = (\gamma - 1)\rho I$.

Numerical Discretization

The semidiscrete conservation form of the equations is given by

$$(\bar{Q}_{i,j,k})_\tau + \left(\bar{F}_{i+\frac{1}{2},j,k} - \bar{F}_{i-\frac{1}{2},j,k}\right) + \left(\bar{G}_{i,j+\frac{1}{2},k} - \bar{G}_{i,j-\frac{1}{2},k}\right) + \left(\bar{H}_{i,j,k+\frac{1}{2}} - \bar{H}_{i,j,k-\frac{1}{2}}\right) \tag{4}$$

where overbars denote the numerically approximated vectors. A pseudofinite volume framework is obtained by the similarity relation $\bar{Q}_{i,j,k} = Q_{i,j,k}V_{i,j,k}$ for the volume $V_{i,j,k}$. The cell volumes are computed by evaluating a combination of six tetrahedra that it is composed of. The metrics κ_x/J, κ_y/J, and κ_z/J for $\kappa = (\xi, \eta, \zeta)$ are related directly to the cell face normals n_x, n_y, and n_z, respectively.

Numerical Scheme

The numerical scheme employed for the solution of the Euler equations is the upwind, TVD (MUSCL) formulation of Roe's Riemann solver.[1]

We denote the cell face of interest as $m+1/2$ where $m = i, j$, or k for the calculation of fluxes $\bar{F}$, $\bar{G}$, or $\bar{H}$, respectively. The numerical inviscid fluxes are represented collectively as $\bar{E}_{m+1/2}(Q, N)$. The local cell face normal is $N = n_x\hat{i} + n_y\hat{j} + n_z\hat{k}$.

Received March 23, 1994; presented as Paper 94-1875 at the AIAA 12th Applied Aerodynamics Conference, Colorado Springs, CO, June 20–23, 1994; revision received Sept. 29, 1994; accepted for publication Dec. 10, 1994.

*Scientist, Computational and Theoretical Fluid Dynamics Division. Associate Fellow AIAA.

†Research Fellow, Computational and Theoretical Fluid Dynamics Division.

Roe's Riemann Solver

The left state of the cell face of the state vector of conserved variables after the MUSCL preprocessing is $\boldsymbol{Q}^-$ and the state vector to the right of the cell face is $\boldsymbol{Q}^+$. The interface enthalpy, $h = \gamma p/(\gamma - 1)\rho + q^2/2$, in addition to the density and velocity components are used for this purpose. The flux difference scheme, based on Roe's Riemann solver[2] utilizes the following linearization at $m + 1/2$, between the left and right states:

$$\begin{aligned}
\chi &= \sqrt{\rho^+_{m+\frac{1}{2}}/\rho^-_{m+\frac{1}{2}}} \\
\rho_{m+\frac{1}{2}} &= \rho^-_{m+\frac{1}{2}}\chi \\
u_{m+\frac{1}{2}} &= \left(u^+_{m+\frac{1}{2}}\chi + u^-_{m+\frac{1}{2}}\right)/(1+\chi) \\
v_{m+\frac{1}{2}} &= \left(v^+_{m+\frac{1}{2}}\chi + v^-_{m+\frac{1}{2}}\right)/(1+\chi) \\
w_{m+\frac{1}{2}} &= \left(w^+_{m+\frac{1}{2}}\chi + w^-_{m+\frac{1}{2}}\right)/(1+\chi) \\
h_{m+\frac{1}{2}} &= \left(h^+_{m+\frac{1}{2}}\chi + h^-_{m+\frac{1}{2}}\right)/(1+\chi)
\end{aligned} \tag{5}$$

where the acoustic speed at the interface is

$$c_{m+\frac{1}{2}} = \sqrt{\left[h_{m+\frac{1}{2}} - q^2_{m+\frac{1}{2}}/2\right](\gamma - 1)} \tag{6}$$

The Roe linearization satisfies the conservation property for the cell face flux Jacobian

$$\bar{A}_{m+\frac{1}{2}} = \Delta\bar{E}_{m+\frac{1}{2}}/\Delta\bar{Q}_{m+\frac{1}{2}} \tag{7}$$

We obtain the eigenvalues and eigenvectors at the cell face by employing the Roe average values

$$\begin{aligned}
\lambda^i_{m+\frac{1}{2}} &= \lambda^i_{m+\frac{1}{2}}\left(Q_{m+\frac{1}{2}}, N_{m+\frac{1}{2}}\right) \\
l^i_{m+\frac{1}{2}} &= l^i_{m+\frac{1}{2}}\left(Q_{m+\frac{1}{2}}, N_{m+\frac{1}{2}}\right) \\
r^i_{m+\frac{1}{2}} &= r^i_{m+\frac{1}{2}}\left(Q_{m+\frac{1}{2}}, N_{m+\frac{1}{2}}\right)
\end{aligned} \tag{8}$$

At every cell face we define the positive and negative components of the eigenvalues by

$$\lambda^{i\pm} = \left(\lambda^i_{m+\frac{1}{2}} \pm \left|\lambda^i_{m+\frac{1}{2}}\right|\right)/2, \qquad i = 1, \ldots, 5 \tag{9}$$

Roe's Riemann solver yields spurious nonphysical phenomena such as expansion shocks at sonic rarefactions. This has to be modified by added dissipation at these locations by employing an entropy fix that circumvents the pitfalls of Roe's method.

The eigenvalues are given by

$$\begin{aligned}
\lambda^1 &= \bar{W} - c\sqrt{n_x^2 + n_y^2 + n_z^2} \\
\lambda^{2,3,4} &= \bar{W} \\
\lambda^5 &= \bar{W} + c\sqrt{n_x^2 + n_y^2 + n_z^2}
\end{aligned} \tag{10}$$

where

$$\bar{W} = \frac{1}{J}W = U \cdot N \tag{11}$$

The numerical flux for the scheme $\bar{E}_{m+1/2}$ is given by the general formulation

$$\bar{E}_{m+\frac{1}{2}} = \tfrac{1}{2}\left[\bar{E}\left(Q^+_{m+\frac{1}{2}}, N_{m+\frac{1}{2}}\right) + \bar{E}\left(Q^-_{m+\frac{1}{2}}, N_{m+\frac{1}{2}}\right)\right] - \frac{1}{2}\left[\sum_i \left|\lambda^i_{m+\frac{1}{2}}\right|\alpha^i_{m+\frac{1}{2}} r^i_{m+\frac{1}{2}}\right] \tag{12}$$

where the characteristic vector $\alpha^i_{m+1/2}$ is obtained as

$$\alpha^i_{m+\frac{1}{2}} = l^i_{m+\frac{1}{2}}\left(Q^+_{m+\frac{1}{2}} - Q^-_{m+\frac{1}{2}}\right) \tag{13}$$

TVD (MUSCL) Formulation

The higher order MUSCL interpolation for the characteristic vectors is obtained as follows. The following variables for state vector of characteristic variables are defined to obtain the left-cell-face state vector of conserved variables $Q^-_{m+1/2}$ as derived later in this section:

$$\begin{aligned}
\overleftarrow{\alpha}^i_m &= l^i_m(Q_m - Q_{m-1}) \\
\vec{\alpha}^i_m &= l^i_m(Q_{m+1} - Q_m)
\end{aligned} \tag{14}$$

We obtain the right-cell-face state vector of conserved variables $Q^+_{m+1/2}$ by defining

$$\begin{aligned}
\overleftarrow{\alpha}^i_{m+1} &= l^i_{m+1}(Q_{m+1} - Q_m) \\
\vec{\alpha}^i_{m+1} &= l^i_{m+1}(Q_{m+2} - Q_{m+1})
\end{aligned} \tag{15}$$

where the ith left eigenvector at the cell m is given by

$$l^i_m = l^i\left[Q_m, \left(N_{m+\frac{1}{2}} + N_{m-\frac{1}{2}}\right)/2\right] \tag{16}$$

The ith right eigenvector at the cell m is given by

$$r^i_m = r^i\left[Q_m, \left(N_{m+\frac{1}{2}} + N_{m-\frac{1}{2}}\right)/2\right] \tag{17}$$

From the definitions the MUSCL preprocessing yields the left and right state vectors of cell face $m + 1/2$

$$\begin{aligned}
Q^-_{m+\frac{1}{2}} &= Q_m + \sum_i \left(\frac{1+\phi}{4}\vec{\beta}^i_m + \frac{1-\phi}{4}\overleftarrow{\beta}^i_m\right) r^i_m \\
Q^+_{m+\frac{1}{2}} &= Q_{m+1} - \sum_i \left(\frac{1+\phi}{4}\vec{\beta}^i_{m+1} + \frac{1-\phi}{4}\overleftarrow{\beta}^i_{m+1}\right) r^i_{m+1}
\end{aligned} \tag{18}$$

The vector $\overleftarrow{\beta}^i_m$ and $\vec{\beta}^i_m$ are obtained from the vectors $\overleftarrow{\alpha}^i_m$ and $\vec{\alpha}^i_m$ and the vectors $\overleftarrow{\beta}^i_{m+1}$ and $\vec{\beta}^i_{m+1}$ are obtained from the vectors $\overleftarrow{\alpha}^i_{m+1}$ and $\vec{\alpha}^i_{m+1}$ by using TVD limiters. At maxima or minima the overall scheme reduces to first order. In the present study, the second-order fully upwind formulation, i.e., $\phi = -1$ has been employed throughout.

The interpolated values now represent the left and right states of Roe's Riemann solver. We will refer to $Q^-_{m+1/2}$ and $Q^+_{m+1/2}$ as Q_L and Q_R alternatively. Various limiters are available to determine the vectors $\overleftarrow{\beta}^i_m$ and $\vec{\beta}^i_{m+1}$. Note that $\vec{\beta}^i_m$ and $\vec{\beta}^i_{m+1}$ drop out for the fully upwind scheme.

TVD Limiters

A large number of TVD limiters have been used to develop high-resolution schemes and have been studied for simple one-dimensional and two-dimensional problems.[4–8] A detailed three-dimensional numerical study of some of the popular limiters has been attempted by the authors in the present work. The sections to follow describe various limiters formulated for a uniform mesh and the corresponding modifications, depending on cell distances, for a nonuniform mesh.[3] The limiters are generally defined in terms of the function

$$\hat{\gamma} = \overleftarrow{\alpha}^i_m/\vec{\alpha}^i_m \tag{19}$$

The nonuniformity of the mesh is taken into account by defining the cell center distances. The position vectors to the cell centroid are defined in terms of the vector s. We define the following distances:

$$\begin{aligned}
\overleftarrow{S}_m &= |s_m - s_{m-1}| \\
\vec{S}_m &= |s_{m+1} - s_m| \\
\overleftarrow{S}_{m+1} &= |s_{m+1} - s_m| \\
\vec{S}_{m+1} &= |s_{m+2} - s_{m+1}|
\end{aligned} \tag{20}$$

Chakravarthy–Osher Limiter

This limiter is also called the minmod limiter. The formulation for the Chakravarthy–Osher limiter[1] is given by the limiter function of the form

$$\sigma(\hat{r}) = \text{minmod}(\hat{r}, \psi) \tag{21}$$

where the minmod function is given by

$$\text{minmod}[x, y] = \text{sign}(x)\max\{0, \min[|x|, y\,\text{sign}(x)]\} \tag{22}$$

and the compression parameter ψ is

$$1 \le \psi \le (3-\phi)/(1-\phi) \tag{23}$$

We obtain the vectors in Eq. (18) using the minmod limiter as follows:

$$\begin{aligned} \vec{\beta}^i_m &= \text{minmod}\left(\overleftarrow{\alpha}^i_m, \psi\vec{\alpha}^i_m\right) \\ \vec{\beta}^i_{m+1} &= \text{minmod}\left(\vec{\alpha}^i_{m+1}, \psi\,\overleftarrow{\alpha}^i_{m+1}\right) \end{aligned} \tag{24}$$

The corresponding formulation for a nonuniform mesh is as follows:

$$\begin{aligned} \vec{\beta}^i_m &= \text{minmod}\left[(\vec{S}_m/\overleftarrow{S}_m)\,\overleftarrow{\alpha}^i_m, \psi\vec{\alpha}^i_m\right] \\ \vec{\beta}^i_{m+1} &= \text{minmod}\left[(\overleftarrow{S}_{m+1}/\vec{S}_{m+1})\vec{\alpha}^i_{m+1}, \psi\,\overleftarrow{\alpha}^i_{m+1}\right] \end{aligned} \tag{25}$$

Roe Diffusive Limiter

The Roe diffusive limiter[1,4] is the most diffusive of all of the limiters studied by the authors and is obtained by setting the compression parameter ψ in Eq. (23) to 1. The formulation for this limiter then follows from the limiter already described.

Van Albada Limiter

The van Albada limiter[5] is formally defined by the function

$$\sigma(\hat{r}) = \frac{\hat{r} + |\hat{r}|}{1 + \hat{r}^2} \tag{26}$$

We define the slopes $\Delta\alpha^i_m$ and $\Delta\alpha^i_{m+1}$ as

$$\begin{aligned} \Delta\alpha^i_m &= \text{sign}\left(\vec{\alpha}^i_m\right)\min\left(\left|\overleftarrow{\alpha}^i_m\right|, \left|\vec{\alpha}^i_m\right|\right) \\ \Delta\alpha^i_{m+1} &= \text{sign}\left(\overleftarrow{\alpha}^i_{m+1}\right)\min\left(\left|\vec{\alpha}^i_{m+1}\right|, \left|\overleftarrow{\alpha}^i_{m+1}\right|\right) \end{aligned} \tag{27}$$

which are then treated by using the limiter function. The function defined for the ith characteristic vector is given by

$$\sigma^i_m = \frac{\overleftarrow{\alpha}^i_m\vec{\alpha}^i_m + \left|\overleftarrow{\alpha}^i_m\vec{\alpha}^i_m\right|}{\left(\overleftarrow{\alpha}^i_m\right)^2 + \left(\vec{\alpha}^i_m\right)^2 + \epsilon} \tag{28}$$

where ϵ is a small number which prevents division by zero and $0 \le \sigma^i_m \le 1$.

The nonuniformity of the mesh is treated by modifying the slope in Eq. (27):

$$\begin{aligned} \Delta\alpha^i_m &= \text{sign}\left(\vec{\alpha}^i_m\right)\min\left(\left|\frac{\vec{S}_m}{\overleftarrow{S}_m}\overleftarrow{\alpha}^i_m\right|, \left|\vec{\alpha}^i_m\right|\right) \\ \Delta\alpha^i_{m+1} &= \text{sign}\left(\overleftarrow{\alpha}^i_{m+1}\right)\min\left(\left|\frac{\overleftarrow{S}_{m+1}}{\vec{S}_{m+1}}\vec{\alpha}^i_{m+1}\right|, \left|\overleftarrow{\alpha}^i_{m+1}\right|\right) \end{aligned} \tag{29}$$

The limiter function in Eq. (28) is modified as

$$\sigma^i_m = \frac{\left(\overleftarrow{\alpha}^i_m/\overleftarrow{S}_m\right)\left(\vec{\alpha}^i_m/\vec{S}_m\right) + \left|\left(\overleftarrow{\alpha}^i_m/\overleftarrow{S}_m\right)\left(\vec{\alpha}^i_m/\vec{S}_m\right)\right|}{\left(\overleftarrow{\alpha}^i_m/\overleftarrow{S}_m\right)^2 + \left(\vec{\alpha}^i_m/\vec{S}_m\right)^2 + \epsilon} \tag{30}$$

where the variable $\hat{r}$ for a nonuniform mesh can be defined as

$$\hat{r} = \frac{\left(\overleftarrow{\alpha}^i_m/\overleftarrow{S}_m\right)}{\left(\vec{\alpha}^i_m/\vec{S}_m\right)} \tag{31}$$

We then obtain the slope with limiters, Eq. (18), by using the formulation for a uniform mesh given by Eqs. (27) and (28) or for a nonuniform mesh given by Eqs. (29) and (30):

$$\begin{aligned} \vec{\beta}^i_m &= \sigma^i_m\Delta\alpha^i_m \\ \vec{\beta}^i_{m+1} &= \sigma^i_{m+1}\Delta\alpha^i_{m+1} \end{aligned} \tag{32}$$

which reduces to zero at local maxima or minima.

Van Leer Limiter

The van Leer limiter[6] is given by the function

$$\sigma(\hat{r}) = \frac{\hat{r} + |\hat{r}|}{1 + |\hat{r}|} \tag{33}$$

The limiter for the ith characteristic vector is defined by

$$\sigma^i_m = \frac{\overleftarrow{\alpha}^i_m\left|\vec{\alpha}^i_m\right| + \vec{\alpha}^i_m\left|\overleftarrow{\alpha}^i_m\right|}{\vec{\alpha}^i_m\left|\vec{\alpha}^i_m\right| + \vec{\alpha}^i_m\left|\overleftarrow{\alpha}^i_m\right| + \epsilon} \tag{34}$$

This limiter is modified for nonuniform meshes as

$$\sigma^i_m = \frac{\left(\overleftarrow{\alpha}^i_m/\overleftarrow{S}_m\right)\left|\left(\vec{\alpha}^i_m/\vec{S}_m\right)\right| + \left(\vec{\alpha}^i_m/\vec{S}_m\right)\left|\left(\overleftarrow{\alpha}^i_m/\overleftarrow{S}_m\right)\right|}{\left(\vec{\alpha}^i_m/\vec{S}_m\right)\left|\left(\vec{\alpha}^i_m/\vec{S}_m\right)\right| + \left(\vec{\alpha}^i_m/\vec{S}_m\right)\left|\left(\overleftarrow{\alpha}^i_m/\overleftarrow{S}_m\right)\right| + \epsilon} \tag{35}$$

where the expression for $\hat{r}$ when considering a nonuniform mesh is given by Eq. (31).

The corresponding limiter functions for uniform and nonuniform meshes are given by Eq. (34) and Eq. (35), respectively. The corresponding slopes are defined by Eq. (27) and Eq. (29). We then obtain the slope limited functions in Eq. (18) by the relation used in Eq. (32).

Roe Superbee Limiter

The functional form of the Roe superbee limiter[7] is given by

$$\sigma(\hat{r}) = \text{superbee}(\hat{r}, 1) \tag{36}$$

where we define the function superbee as

$$\text{superbee}(x, y) = \max[0, \min(2x, y), \min(x, 2y)] \tag{37}$$

We obtain the variable vectors in Eq. (18) using the superbee limiter as follows.

$$\begin{aligned} \vec{\beta}^i_m &= \text{superbee}\left(\overleftarrow{\alpha}^i_m, \vec{\alpha}^i_m\right) \\ \vec{\beta}^i_{m+1} &= \text{superbee}\left(\vec{\alpha}^i_{m+1}, \overleftarrow{\alpha}^i_{m+1}\right) \end{aligned} \tag{38}$$

The nonuniformity of the mesh is taken into account by changing the formulation as

$$\begin{aligned} \vec{\beta}^i_m &= \text{superbee}\left(\left(\vec{S}_m/\overleftarrow{S}_m\right)\overleftarrow{\alpha}^i_m, \vec{\alpha}^i_m\right) \\ \vec{\beta}^i_{m+1} &= \text{superbee}\left(\left(\overleftarrow{S}_{m+1}/\vec{S}_{m+1}\right)\vec{\alpha}^i_{m+1}, \overleftarrow{\alpha}^i_{m+1}\right) \end{aligned} \tag{39}$$

Davis Limiter

The Davis limiter[8] is defined by the function

$$\sigma(\hat{r}) = \text{minmod}(2\hat{r}, 1) \tag{40}$$

The minmod limiter is defined in Eq. (22).

The implementation for uniform meshes is

$$\begin{aligned} \vec{\beta}^i_m &= \text{minmod}\left(2\,\overleftarrow{\alpha}^i_m, \vec{\alpha}^i_m\right) \\ \vec{\beta}^i_{m+1} &= \text{minmod}\left(2\vec{\alpha}^i_{m+1}, \overleftarrow{\alpha}^i_{m+1}\right) \end{aligned} \tag{41}$$

The formulation for a nonuniform mesh is given by

$$\overleftarrow{\beta}^i_m = \text{minmod}\left(2(\vec{S}_m/\overleftarrow{S}_m)\overleftarrow{\alpha}^i_m, \vec{\alpha}^i_m\right)$$
$$\overleftarrow{\beta}^i_{m+1} = \text{minmod}\left(2(\overleftarrow{S}_{m+1}/\vec{S}_{m+1})\vec{\alpha}^i_{m+1}, \overleftarrow{\alpha}^i_{m+1}\right) \quad (42)$$

Entropy Fix

The main drawback in the Roe linearization is the violation of entropy at sonic rarefractions. These are not the only problems faced by this method. Quirk[9] has illustrated various other pitfalls; the formation of Carbuncle shocks, strong odd-even coupling of pressure and density resulting in the breakdown of grid aligned planar shocks, negative internal energies, kinked Mach stems, and inability to resolve slow moving shocks. Furthermore, it was noted by Quirk that Harten's entropy fix and its variants invariably cure these when the fixes are also applied to the linear waves. The entropy fixes studied in the present work are by Chakravarthy[1] and three variants of the basic Harten fix.[10–12] These fixes are applied to all of the waves.

Chakravarthy Entropy Fix

In the original formulation a correction is applied only at the sonic rarefactions, $[\lambda^i(\boldsymbol{Q}_m, \boldsymbol{N}_{m+1/2}) < 0 < \lambda^i(\boldsymbol{Q}_{m+1}, \boldsymbol{N}_{m+1/2})]$, but we have applied the entropy fix to all of the waves. This is given by correcting the eigenvalue spectrum as follows:

$$\lambda^{i\pm}_{m+\frac{1}{2}} = \lambda^{i\pm}_{m+\frac{1}{2}} \pm \left[\lambda\left(\boldsymbol{Q}^i_{m+1}, \boldsymbol{N}_{m+\frac{1}{2}}\right) - \lambda\left(\boldsymbol{Q}^i_m, \boldsymbol{N}_{m+\frac{1}{2}}\right)\right]/4 \quad (43)$$

where the latter term in brackets represent the added dissipation.

Harten/Harten–Yee Entropy Fix

The general form of Harten's entropy fix is given by Harten[10]:

$$|\lambda| = \begin{cases} |\lambda|, & \text{if } |\lambda| \geq \delta \\ (\lambda^2 + \delta^2)/(2\delta), & \text{if } |\lambda| < \delta \end{cases} \quad (44)$$

where $0.05 \leq \delta \leq 0.25$. Variants to the basic Harten's entropy fix have been developed depending on how δ is specified.

A study by Yee[11] demonstrates that δ has to be modified for hypersonic flows as follows:

$$\delta = \delta^*\left[\left|\bar{W}^\xi_{m+\frac{1}{2}}\right| + \left|\bar{W}^\eta_{m+\frac{1}{2}}\right| + \left|\bar{W}^\zeta_{m+\frac{1}{2}}\right| + \frac{1}{3}c\left(\left|\nabla\frac{\xi}{J}\right| + \left|\nabla\frac{\eta}{J}\right| + \left|\nabla\frac{\zeta}{J}\right|\right)\right] \quad (45)$$

where $\bar{W}^\xi$, $\bar{W}^\eta$, and $\bar{W}^\zeta$ are the contravariant velocities in the ξ, η, and ζ directions, respectively, and $0.05 \leq \delta^* \leq 0.25$.

Harten–Hyman Entropy Fix

The following entropy fix due to Harten and Hyman[12] relates the entropy fix to average state between the left and right states of the interface. This is a variant of the basic Harten's entropy fix. The entropy fix parameter δ in Eq. (44) is now given by

$$\delta = \max\left[0, \left\{\lambda^i(\boldsymbol{Q}_L, \boldsymbol{Q}_R) - \lambda^i(\boldsymbol{Q}_L, \boldsymbol{Q}(\theta)\right]\right\} \left\{\lambda^i[\boldsymbol{Q}(\theta), \boldsymbol{Q}_R] - \lambda^i(\boldsymbol{Q}_L, \boldsymbol{Q}_R)\right\}\right] \quad (46)$$

where $\lambda^i(a, b)$ is the eigenvalue obtained from the Roe-averaged value of the left and right states (a, b). In Eq. (46) the vector $Q(\theta)$ is given by

$$\boldsymbol{Q}(\theta) = \boldsymbol{Q}_L + \theta(\boldsymbol{Q}_R - \boldsymbol{Q}_L)$$

for $0 \leq \theta \leq 1$. A constant θ of 0.5 has been used in the present study.

Boundary Conditions

The following boundary conditions have been used:

Inflow and Supersonic Outflow Boundary

Freestream conditions have been imposed at the inflow boundary. A two cell specification at the inflow boundary takes care of the high-resolution scheme. At the outflow a first-order extrapolation in the streamwise—ξ direction is implemented as

$$\frac{\partial^2 \boldsymbol{Q}}{\partial \xi^2} = 0 \quad (47)$$

Wall Boundary

We obtain the right state at the wall, denoted by the R-subscripted values, by extrapolating from the interior of the flowfield. The wall boundary conditions are imposed by the exact solution of the one-sided Riemann problem:

$$(p/\rho^\gamma)_W = (p/\rho^\gamma)_R$$
$$\left(u - \frac{2}{\gamma - 1}c\right)_W = \left(u - \frac{2}{\gamma - 1}c\right)_R \quad (48)$$

where the subscript W represents the wall conditions. Since the Euler wall boundary condition implies zero normal velocity, the one-dimensional solution procedure just given results in $u_W = 0$.

From Eqs. (48), we get

$$p_W = p_R\left(1 - \frac{\gamma - 1}{2}\frac{u_R}{c_R}\right)^{2\gamma/(\gamma-1)} \quad (49)$$

Since the scheme is second-order accurate, we create a ghost cell next to the wall and obtain values therein by reflection.

Grid Singularity Treatment

The three-dimensional axisymmetric grid is generated by rotating a two-dimensional grid by 360 deg. This generates an axial singularity where the surface collapses into a line. This is treated in the present study by merging all of the pyramid cells adjoining the singular line into a larger cell which looks like a frustrum of a cone with an outer polyhedral surface. The flux balance across this cell is treated by considering the outgoing flux across all of the polyhedral surfaces and, thus, circumventing the problem of considering the physical nature of flux across a singularity.

Test Cases and Grid Generation

The two test cases employed for the study of supersonic and hypersonic blunt body flows are as follows: 1) supersonic flow over a hemisphere-cylinder at a freestream Mach number of 2.94 and zero angle of attack (case 1) and 2) hypersonic flow over a hemisphere cone (semicone angle of 15 deg) at a freestream Mach number of 10.6 and an angle of attack of 15 deg (case 2).

An algebraic grid generator with uniform cell spacing normal to the wall and streamwise stretching along the cylinder/cone has been used (Fig. 1). A uniform spacing in the circumferential direction is employed.

The grid size in the ξ, η, and ζ directions for both case 1 and case 2 is $(25 \times 19 \times 20)$. These are the streamwise direction, the direction normal to the wall, and the crosswise direction, respectively.

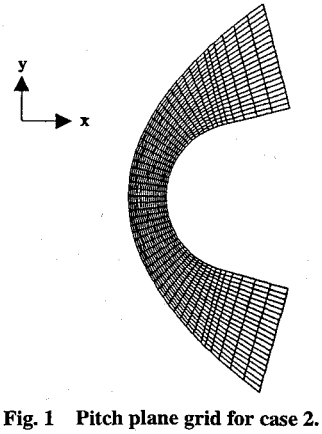

Fig. 1 Pitch plane grid for case 2.

It will be shown later that even this crude grid definition provided accurate results.

Parallelization Technique

The computer code was implemented on the Flosolver MK3, a parallel machine based on the Intel i860 chip and developed at the National Aerospace Laboratories, Bangalore, India. The Flosolver has a master processor called the Host that takes care of the I/O and slave processors, designated as PE, which in conjunction with the Host are used for number crunching. A maximum of 16 simultaneous processors can be used (6–12 mflops per processor). The procedure used to effect computation is domain decomposition along the streamwise—ξ direction on a 4-node implementation. An overlap of two cells between the neighboring processors is provided to facilitate the second-order implementation of the scheme.

Results and Discussions

This section first considers the effect of using nonlinear interpolation in TVD limiters. Next, a comparative study of entropy fixes is provided. This is followed by a comparative study of limiters, which includes Mach number dependence and grid sensitivity studies. The accuracy of shock resolution inherent in the scheme is then presented. Finally, the results of the computed flowfield for case 1 and case 2 are presented and discussed.

Nonlinear Interpolation

Case 2 (hypersonic flow) has been chosen for this study. Here the limiters which take into account mesh spacing will be referred to as scaled, whereas those without mesh spacing as unscaled. The entropy fix due to Harten–Yee and the Roe diffusive limiter have been used in this study. The inclusion of mesh spacing in the formulation of the TVD limiter results in a dramatic improvement in the convergence characteristics (Fig. 2).

The limiter functions basically involve gradients of a flow parameter. When the mesh is nonuniform it is important to take into account the mesh spacing for accurate implementation of these gradients in the MUSCL interpolation. Otherwise, this may result in local interpolation errors in the MUSCL approach with adverse effect on global convergence. In the test cases considered, the parameter scaling did not show any significant effect on the shock resolution nor on surface pressure distribution.

All of the results presented next involve the use of limiters with nonlinear interpolation involving mesh spacing.

Comparative Study of Entropy Fixes

The performance of three entropy fixes, Chakravarthy, Harten, and Harten–Hyman, is compared in terms of convergence characteristics in Fig. 3 for case 1. An improved convergence is obtained for Harten's fix where δ in Eq. (44) was set at 0.125. The performance of the other two fixes is similar. It was observed that the choice of the entropy fix does not have any significant effect on the accuracy of the computations.

The entropy fixes mentioned work satisfactorily for supersonic flows but do not provide proper convergence for hypersonic flow computations (case 2). Furthermore, the hypersonic flow case does show the occurrence of the carbuncle phenomenon and expansion shocks, although not presented here, when computed with Chakravarthy and Harten–Hyman entropy fix. The Harten–Yee modification of the basic Harten's entropy fix has been found to be quite robust for hypersonic flow computations. The value of δ^* in Eq. (45) used in these computations was 0.15.

The present study thus shows that the observation by Quirk[9] that most of the shortcomings of Roe's scheme for high-speed blunt body flow computations are invariably overcome by employing the Harten/Harten–Yee entropy fix is valid even for three-dimensional flows.

Comparative Study of Limiters

The various formulation of limiters are tested on the case 2 (hypersonic flow) with entropy fix due to Harten–Yee and their performance compared in terms of convergence in Fig. 4. It may be observed that for the coarse grid employed here, the performance

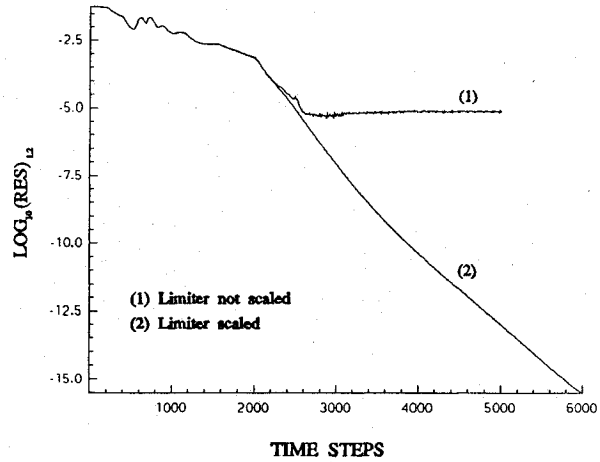

Fig. 2 Effect of nonlinear interpolation on TVD limiters for case 2.

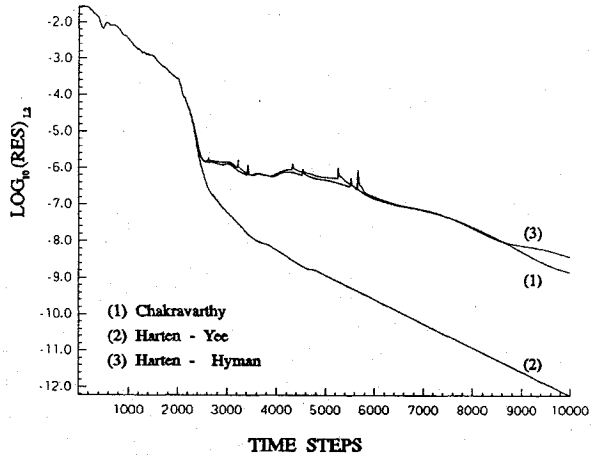

Fig. 3 Comparison of various entropy fixes for case 1.

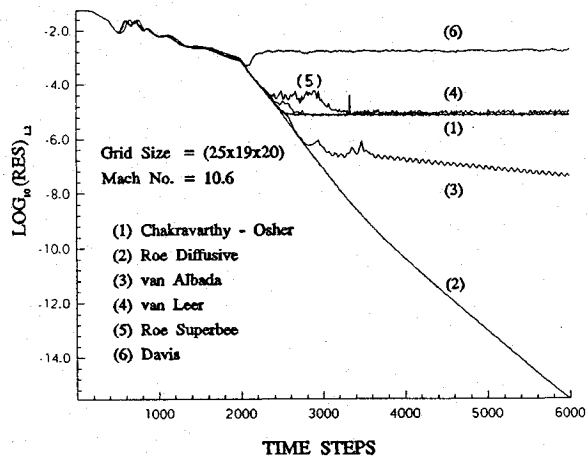

Fig. 4 Comparison of various TVD limiters for case 2.

of the TVD limiters is a monotonic function of their diffusivity. The Roe diffusive limiter (most diffusive) provides the best convergence, whereas the Davis limiter (least diffusive) performs rather poorly. The effect of Mach number and grid sensitivity on limiters is studied in the following section with Fig. 4 as its basis.

Mach Number Dependence and Grid Sensitivity Studies

These studies demonstrate the effect of Mach number and grid refinement on the convergence behavior of limiters. The test case 2 has been used as the basis for this study. The geometry and angle of attack for the study remains the same. Because of limited computational resources available we restrict the study to three limiters, Roe diffusive, van Albada, and van Leer. These are in order of decreasing

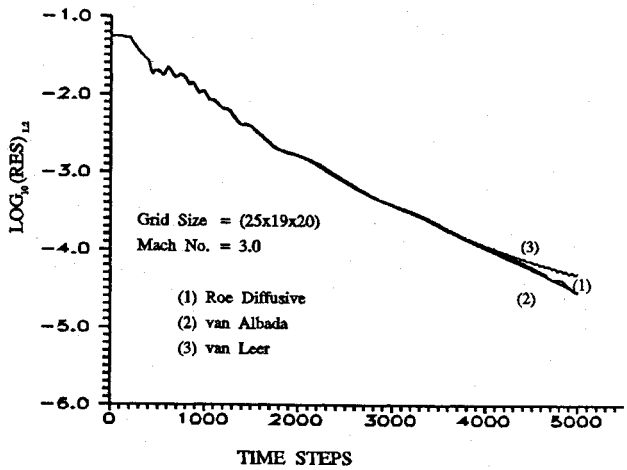

Fig. 5 Mach number dependence study on TVD limiters for case 2 configuration.

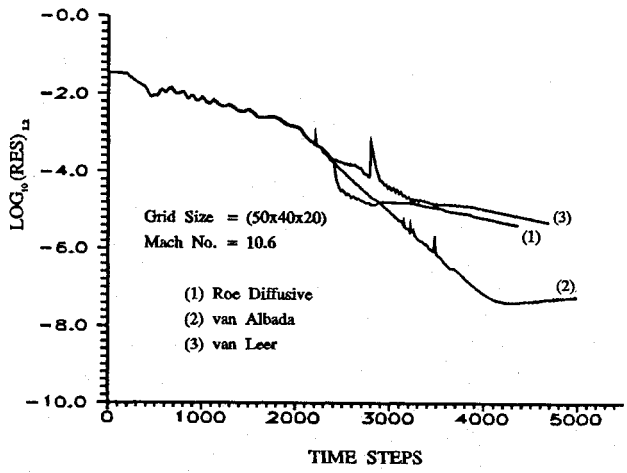

Fig. 6 Grid sensitivity study on TVD limiters for case 2 configuration.

diffusive characteristics[4] with the van Leer limiter being the most compressive of the three.

The Mach number dependence is studied by using the same grid as in case 2 with a freestream Mach number of 3 instead of 10.6. The convergence characteristics are shown in Fig. 5.

The grid sensitivity is studied by refining the pitchplane grid definition from 25×19 in case 2 to 50×40. The Mach number remains unaltered. The convergence characteristics are shown in Fig. 6.

A comparative study of Figs. 4–6 demonstrates the following results. At the supersonic Mach number, the limiters show almost the same convergence characteristics (Fig. 5). At the hypersonic speed, the performance of the limiters seems to differ. The Roe diffusive limiter appears to be superior to the rest for the coarse grid (Fig. 4), whereas the van Albada limiter seems to perform better on the fine grid (Fig. 6).

Accuracy of Shock Resolution

A comparison of pressure distribution along the stagnation line demonstrates the accuracies involved in shock resolution. Figure 7 shows the stagnation line pressure distribution at Mach 3 and a coarse grid definition of $(25 \times 19 \times 20)$ for the hemisphere cone (case 2 configuration). Figure 8 shows the pressure distribution for the same configuration at Mach 10.6 and a fine grid definition $(50 \times 40 \times 20)$.

We note that the three limiters show the same two-point shock structure irrespective of the grid refinement and Mach number. As the grid gets refined, these points across the shock will be closely clustered and, hence, provide a sharper description of the shock. Futhermore, it can be seen that the stagnation pressure is computed to a very high degree of accuracy in all of the cases.

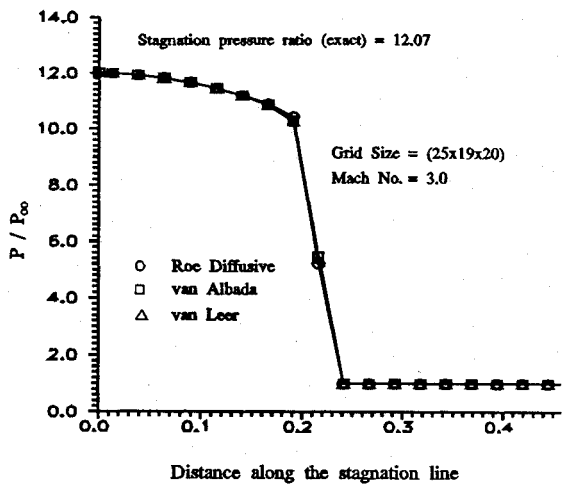

Fig. 7 Pressure distribution along stagnation line for the Mach number dependency study.

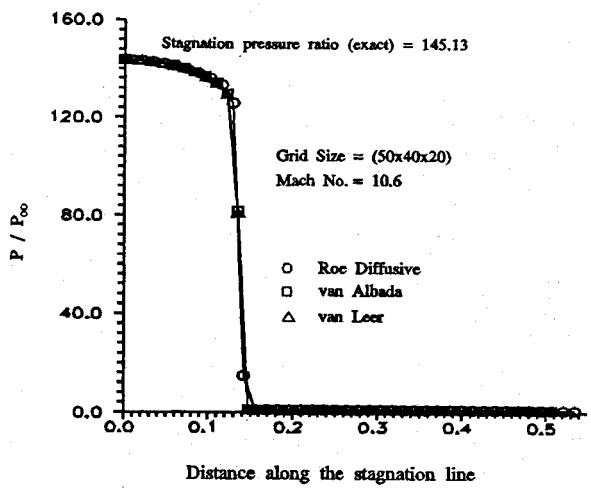

Fig. 8 Pressure distribution along stagnation line for the grid sensitivity study.

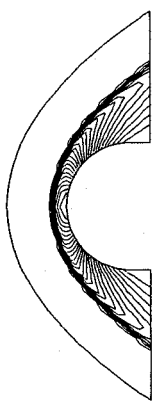

Fig. 9 Density contours in the pitch plane for case 1.

Computed Flowfield

All of the flowfield results presented have the Roe diffusive limiter for the high-resolution scheme. The entropy fix used is the Harten's fix for the case 1 and the Harten–Yee extension of the Harten's fix for case 2.

The density contours for case 1 are shown in Fig. 9. The shock is resolved accurately even on the crude grid used. The computed pressure distribution over the body is shown in Fig. 10 and compares well with the computation due to Viviand and Ghazzi.[13]

The hypersonic case 2 is studied next. The pressure contours are given in Fig. 11. The computed coefficient of pressure on the body is shown in Fig. 12. The comparison in this figure is made

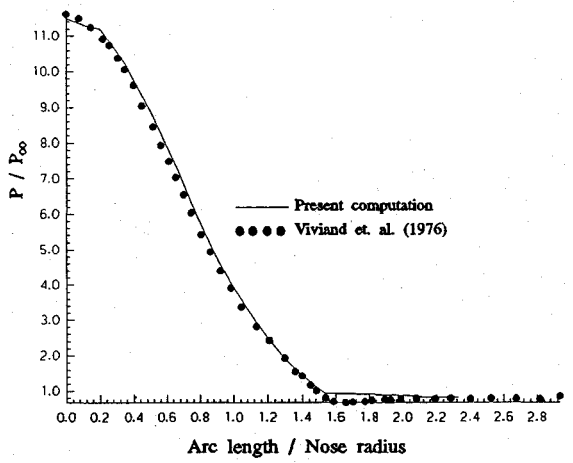

Fig. 10 Pressure distribution along the wall for case 1.

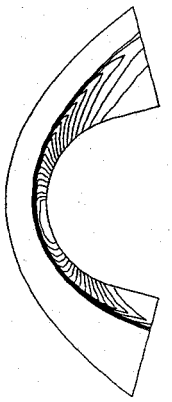

Fig. 11 Pressure contours in the pitch plane for case 2.

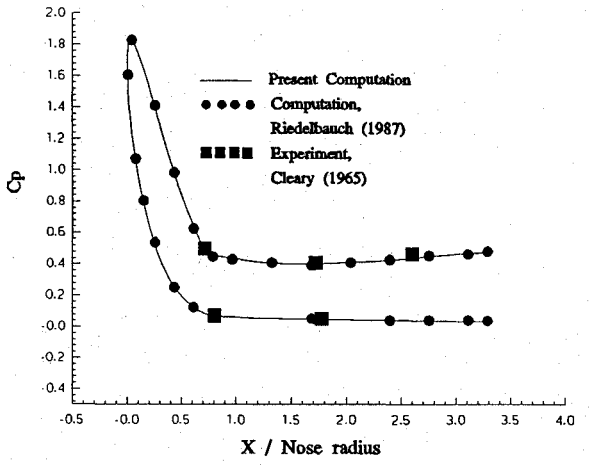

Fig. 12 Pressure distribution along the wall for case 2.

with the experimental study by Cleary[14] and computational work by Riedelbauch and Müller.[15] The accuracy of the overall scheme for both the supersonic test case (case 1) and the hypersonic test case (case 2) has been demonstrated by the surface pressure results in Figs. 10 and 12, respectively.

Concluding Remarks

A flow solver for the solution of three-dimensional Euler equations to compute supersonic and hypersonic blunt body flows has been developed based on an upwind TVD (MUSCL) formulation of the Roe's method. A compatible wall boundary condition procedure with a special treatment of the singularity line for axisymmetric blunt bodies enhances the robustness of the flow solver.

A comparative study of various limiters and entropy fixes has been done to identify the most appropriate combination of the limiter and the entropy fix for the Mach number range of interest. The choice of limiters has an important effect on the convergence characteristics of the flow computations. Furthermore, the robustness of the solver is dictated by the appropriate choice of limiter and entropy fix. The inclusion of cell distances to account for mesh nonuniformity in the limiter formulation shows a dramatic improvement in the convergence characteristics. The Mach number dependence and grid refinement studies carried out in the present work indicate that at supersonic Mach numbers, the performance of the limiters do not significantly differ in terms of convergence. At hypersonic Mach numbers, however, this is not so. The Roe diffusive limiter appears to be superior for coarse grids whereas the van Albada limiter performs better on the fine grids. No matter which TVD limiter is used, the Roe scheme provides the same two-point shock structure irrespective of the Mach number and grid refinement. The accuracy of the computations is not significantly affected for both the supersonic and hypersonic Mach number test cases. The Harten–Yee entropy fix performs consistently well for both these test cases with no spurious solutions such as carbuncle and expansion shocks. The computed results compare well with the available computational and experimental data. Local time stepping and the parallelization technique have enhanced convergence in terms of effective wall clock times.

Acknowledgments

We thank T. S. Prahlad, Coordinator, Aerodynamics Panel, for making this study possible through an AR & DB Project CF-1-121. The present study was carried out in response to a request from DRDL, Hyderabad. Many useful discussions with S. M. Deshpande and S. S. Desai are acknowledged with thanks. Thanks are due to U. N. Sinha and his team at the FLOSOLVER Laboratory for their initial help in the parallelization of the code and usage of the FLOSOLVER machine.

References

[1]Chakravarthy, S. R., "High Resolution Upwind Formulations for the Navier–Stokes Equations," *Computational Fluid Dynamics*, Von Kármán Inst., Lecture Series, 1988-05, 1988.

[2]Roe, P. L., "Approximate Riemann Solvers, Parameter Vectors, and Difference Schemes," *Journal of Computational Physics*, Vol. 43, 1981, pp. 357–372.

[3]Turkel, E., "Accuracy of Schemes with Nonuniform Meshes for Compressible Flows," Inst. for Computer Applications in Science and Engineering, ICASE Rept. 85-43, 1985.

[4]Sweby, P. K., "High Resolution Schemes Using Flux Limiters for Hyperbolic Conservation Laws," *SIAM Journal of Numerical Analysis*, Vol. 21, 1984, pp. 995–1011.

[5]Van Albada, G. D., van Leer, B., and Roberts, W. W., "A Comparative Study of Computational Methods in Cosmic Gas Dynamics," *Astronomy and Astrophysics*, Vol. 108, 1982, pp. 76–84.

[6]Van Leer, B., "Towards the Ultimate Conservative Difference Scheme, II. Monotonicity and Conservation Combined in a Second Order Scheme," *Journal of Computational Physics*, Vol. 14, 1974, pp. 361–370.

[7]Roe, P. L., "Some Contributions to the Modelling of Discontinuous Flows," *Lecture Notes in Applied Mathematics*, Vol. 163, 1985.

[8]Davis, S. F., "TVD Finite Difference Schemes and Artificial Viscocity," Inst. for Computer Applications in Science and Engineering, Tech. Rept. 84-20, June 1984.

[9]Quirk, J. J., "A Contribution to the Great Riemann Solver Debate," NASA CR 191409, Inst. for Computer Applications in Science and Engineering, Rept. 92-64, Nov. 1992.

[10]Harten, A., "On a Class of High Resolution Total-Variation-Stable Finite Difference Schemes," *SIAM Journal of Numerical Analysis*, Vol. 21, 1984, pp. 1–23.

[11]Yee, H. C., "A Class of High-Resolution Explicit and Implicit Shock-Capturing Methods," NASA TM, 101088, Feb. 1989.

[12]Harten, A., and Hyman, J. M., "A Self-Adjusting Grid for the Computation of Weak Solutions of Hyperbolic Conservation Laws," *Journal of Computational Physics*, Vol. 50, 1983, pp. 235–269.

[13]Viviand, H., and Ghazzi, W., "Numerical Solution of the Compressible Navier–Stokes Equations at High Reynolds Number with Applications to the Blunt Body Problem," *Lecture Notes in Physics*, Vol. 59, 1976.

[14]Cleary, J. W., "An Experimental and Theoretical Investigation of the Pressure Distribution and Flow Fields of Blunted Cones at Hypersonic Mach Numbers," NASA TN D-2969, 1965.

[15]Riedelbauch, S. and Müller, B., "The Simulation of Three-Dimensional Viscous Supersonic Flow Past Blunt Bodies with a Hybrid Implicit/Explicit Finite-Difference Method," DFVLR-FB 87-32, 1987.